Research Square

Preprints are preliminary reports that have not undergone peer review.
They should not be considered conclusive, used to inform clinical practice,
or referenced by the media as validated information.

Reduced CXCL1 expression promotes context-dependent tumour aggressiveness in triple-negative breast cancer

Clàudia Martínez Miralles
Universitat Internacional de Catalunya
Evangelos Manousakis
Universitat Internacional de Catalunya
Cristina Moreta-Moraleda
Universitat Internacional de Catalunya
Houda Baccara
University of Parma Department of Chemistry: Universita degli Studi di Parma Dipartimento di Chimica
Luke Mahon
Universitat Internacional de Catalunya
Laia Liñán Franquet
Universitat Internacional de Catalunya
Montserrat Montañes i Albó
Universitat Internacional de Catalunya
Anna Tomás Pujolá
Universitat Internacional de Catalunya
Roberto Ferrari
University of Parma Department of Chemistry: Universita degli Studi di Parma Dipartimento di Chimica
Roni Helene Grace Wright
rhgwright@uic.es

Universitat Internacional de Catalunya https://orcid.org/0000-0002-8194-4614

Research Article

Keywords: triple-negative breast cancer, CXCL1, tumour microenvironment, CAM assay, chemokine, metastasis

Posted Date: September 1st, 2026

DOI: https://doi.org/10.21203/rs.3.rs-10698763/v1

License: This work is licensed under a Creative Commons Attribution 4.0 International License.
Read Full License

Abstract

Triple-negative breast cancer (TNBC) is a highly aggressive breast cancer subtype with limited treatment options. CXCL1 is a proinflammatory chemokine that presents high expression levels in TNBC, yet its precise role remains unclear. In this study, CXCL1 function was studied using TNBC (MDA-MB-231) cell lines. CXCL1 silencing led to a significant increase in invasion, migration and colony formation. *In vivo* analysis using chorioallantoic membrane (CAM) assays supported these findings as CXCL1-silenced tumours were larger and presented apparent enhanced angiogenesis. In addition, patients with low CXCL1 mRNA expression levels present reduced overall survival in TNBC. Single cell analysis linked high CXCL1 expression to inflammatory transcriptional programmes in TNBC epithelial cells. Moreover, spatial transcriptomics showed broad CXCL1 distribution without enrichment of EMT or stemness signatures. These findings reveal a context-dependent tumour-restraining role for CXCL1 in TNBC and support its potential utility as a prognostic biomarker or molecular target in aggressive, metastatic TNBC. Further mechanistic studies are warranted to define the role of CXCL1 in TNBC progression.

INTRODUCTION

Breast cancer is the second most commonly diagnosed cancer (11.6%) and the 4th cancer type mortality worldwide [1]. It comprises several molecular subtypes, including luminal A, luminal B, human epidermal growth factor receptor 2 positive (HER2+) and triple-negative (TNBC) [2]. TNBC is a fast-moving and aggressive subtype with high incidence in young patients and with a high metastatic potential in lungs, brain and lymph nodes [3]. Although dose-dense chemotherapy and targeted strategies against pathways such as PI3K-Akt, MAPK and homologous recombination repair have improved therapeutic options, chemotherapy remains the main treatment and the appearance of metastasis continues to be associated with poor prognosis [3, 4].

Metastasis promotes tumour-promoting inflammation that drives infiltrated immune cells to secrete several factors, such as chemokines, that can facilitate the activation of other hallmarks [5]. In this context, chemokines emerge as key mediators of immune infiltration, inflammation and tumour progression [6]. These secreted proteins are divided into 4 families where CXCL1 belongs to the CXC family and the GRO subgroup, involved in neutrophil recruitment through CXCR2 signalling [7]. In disease, CXCL1 has been described to have an important role for tumour progression through recruiting immune cells [8] and enhancing angiogenesis [9]. In breast cancer, CXCL1 has been defined to promote immunosuppressive TME and lung metastasis [10]. Moreover, it has been linked to therapy resistance in several malignancies such as oesophageal cancer [11] and takes part in complex secretory programmes related to NF-κB and senescence-associated secretory phenotype [12]. Due to its important role in cancer progression, several therapies had been developed targeting CXCR2 such as CXCR2-modified CAR-T cells [13]. Despite CXCL1 appearing to have a general role in neutrophil chemotaxis and inflammation, data from the Breast Invasive Carcinoma TCGA PanCancer collection suggest a correlation between high levels of CXCL1 and triple-negative breast cancer subtype [14]. For this reason,

this study was designed to evaluate the impact of high CXCL1 expression levels in TNBC and its effect *in vitro* and *in vivo.*

MATERIALS AND METHODS

Additional in depth material and methods and company catalog numbers for all products and resources used in this study are provided in supplementary information 2 (SI2).

Multiomics analysis

The DisGeNET database was used for analysing the bibliography-established relation of CXCL1 with non-cancer diseases. The GEPIA2 database was consulted for expression analysis of CXCL1 in different cancer types, subtypes and survival analysis.

The GEO2R tool was used for analysing MDA-MB-231 global RNA sequencing data comparing 2D and 3D cultures (GSE130590).

Both single-cell RNA sequencing and spatial transcriptomics data were retrieved on 6th May 2026 from the publicly available breast cancer atlas generated by Wang, X., Wang, Z., Liao, Q. et al [15]. Data including processed and filtered count matrices, spatial coordinates files, haematoxylin and eosin image data, scale factors were deposited on either Gene Expression Omnibus using the accession GSE176078, or on Zenodo [16]. The dataset included breast cancer samples representing main molecular subtypes such as estrogen receptor positive, HER2-positive and triple-negative breast cancer. Metadata files used for further analysis included patient identifier, breast cancer subtype and major cell type annotations. Both analyses were performed using Google collab version 2026-03-25.

Cell lines and cell culture

Mammalian cancer cell lines MDA-MB-231 and MCF-7 were retrieved from HospitalClínic and Eucellbank repositories and maintained at UIC Barcelona, where they are routinely screened for mycoplasma contamination. Both cell lines were cultured adherent using complete media: Dulbecco's Modified Eagle Medium supplemented with 10% fetal bovine serum (FBS), 1% penicillin-streptomycin (P/S); and 1% glutamine. In 3D cultures, the cells were grown in non-adherent hydrogel coated plates and cultured in DMEM/F-12 supplemented with 10% FBS, 1% P/S, 2% B27 and 20 ng/mL EGF. All cell lines were cultured in a humidified incubator set at 37ºC in a 5% CO_2.

Small Interfering RNA (siRNA) silencing

Cell lines were plated in 6-well plates at a seeding density of $1.5x10^5$ in complete media without antibiotics. Cells were transfected at 70–80% confluence with 100 nM CXCL1-targeting or control siRNA

using Lipofectamine™ 2000 according to the manufacturer's instructions. Two independent CXCL1-targeting siRNAs were used (siCXCL1 and siCXCL1-B).

Gene expression analysis

Total RNA was isolated using the NZY Total RNA Isolation kit according to the manufacturer's instructions. Extract from tissue was previously homogenised using a pestle. Complementary DNA (cDNA) was synthesized with 200 ng of total RNA using High-Capacity cDNA Reverse Transcription Kit following manufacturer's guidelines. Quantitative PCR was performed using SsoAdvanced Universal SYBR® Green Supermix and expression primers sequences used are available in Supplementary Information 3 (SI3 Table 1).

Immunofluorescence

Cells were plated in µ-Slide 8-wells high chambers at a seeding density of $0.3x10^5$. The cells were fixed with 4% Paraformaldehyde for 20 minutes, permeabilized for 15 minutes at RT using 0.1% Triton-X100 and blocked for 30 minutes using 10% BSA. The slide was incubated with a CXCL1 antibody suitable for IF (1:1000) overnight at 4ºC. The secondary antibody used was an Alexa Fluor 488 goat anti-Rabbit (1:1000) incubated for 2 hours at RT in the dark and the mounting media used was antifade mounting media with DAPI. Cells were visualized using Leica Confocal DMi8.

Invasion Assay

24h following siRNA transfection, starved cells were transferred to 8µm pore size and 6.5 mm diameter invasion chambers in starvation media at a seeding density of $1.7\text{-}3.3x10^6$ cells/mL. Each invasion chamber was placed in a 24-well plate containing complete media. After 24-48h, the chambers were washed with PBS and stained with 0.5% crystal violet staining solution diluted in methanol for 15 minutes at room temperature. Excess crystal violet was removed using 1x PBS, invasion chambers were air dried and brightfield images were taken using an EVOS microscope. Images were quantified using ImageJ software.

Wound healing assay

24h post-transfection, scratches were performed in the well using a p1000 and p200 pipette tips. Images were taken at 24, 48 and 72 hours using 10x magnification in an inverted EVOS microscope. Images were analysed using ImageJ.

Colony Assay

500 transfected cells were seeded into 10cm plates and were left to grow in complete media for 20 days. Then, cells were stained using 0.5% crystal violet solution diluted in methanol for 15 minutes at room temperature. Excess crystal violet was removed using 1x PBS or tap water and left to air dry. Images were taken using an EVOS microscope and analysed using ImageJ.

Cell cycle analysis

24h following siRNA transfection, cells were collected in staining solution (10% TritonX-100, 10 mg/mL RNase, 1mg/mL propidium iodide, 20% FBS and PBS) in a proportion of 200uL staining solution each $1.5x10^5$ cells. Samples were incubated on ice in the dark for 10 minutes and propidium iodide was detected by flow-cytometry using Allophycocyanin (APC) channel in a Cytoflex S cytometer. Data was analysed using CytExpert software

Spheroid size and viability assays

Transfected cells were plated in a low-attachment 96-wells U-bottom plate at a seeding density of 100 cells/µL. Images were taken using EVOS microscope after 0, 1, 2, 5 and 6 days. The spheroid size was measured using ImageJ software. LIVE/DEAD™ Viability/Cytotoxicity Kit, for mammalian cells, was used to determine the live and dead percentage of cells according to manufacturer's guidelines. Images were taken using an EVOS microscope and analysed with ImageJ. In parallel, images of spheroids were also taken every 6 hours using Incucyte SX5 for 6 days.

Chorioallantoic membrane (CAM) assays

Fertilized eggs were purchased from a local farm and kept at 4ºC until required. The eggs were cleaned with distilled water, laid horizontally and incubated at 37ºC, 0.5% CO_2 and 70% humidity for 3 days. On day 3, a puncture was performed at the top part of the egg and 3 mL of albumin were removed using a syringe and a 21G needle. On day 6, small windows were carved in the shell and covered with surgical tape. On embryonic developmental day 7, sterile silicone rings were placed in the CAM and $1x10^6$ cells/mL were inoculated on the egg, in the central hole of the silicone ring. The cell suspension was prepared in a 1:1 solution of FBS-Geltrex. Eggs were placed back to the incubator and controlled until EDD14 when tumours and peripheral organs were collected after euthanization of the chicken embryos. Collected tumours were measured using ImageJ.

Vessel density analysis

High resolution images were taken from the silicone rings inner section for each condition. Counting criteria was defined as only clear and defined vessels were considered and vessels were counted in ramification points. Vessels within the region of interest were counted manually following the same criteria. The regions of interest were measured and quantified for normalization using the following equation: $Average\ vessel\ density = \frac{number\ of\ vessels}{region\ of\ interest}$.

Immunohistochemistry

Freshly harvested tissue was fixated in 10% formalin for 24h and then, the tissue was left in 30% sucrose until saturated. Tissue was flash-frozen in isopentane and stored in the − 80ºC until further use. Frozen tissue was embedded in PolyFreeze Tissue Freezing Medium and sectioned at 30 µm using Cryostat. Sections were collected using tweezers and a brush, placed in cryoprotective media, and stored at -20ºC until required. Selected sections were washed with cold 1X KPBS (Vf = 1L; 150 mM NaCl, 8% HK_2PO_4 and 2% H_2KPO_4) and blocked for 1h at RT in KPBS containing 0.1% Triton-X100, 3% Goat serum and 4% BSA. Sections were incubated with the primary antibody diluted in the blocking buffer for 1h RT followed by overnight incubation at 4ºC. After several washes in KPBS containing 0.1% Triton-X100, sections were incubated with Alexa Fluor 568 anti-mouse conjugated secondary antibody (1:1000) for 2h RT. Hoetch 33258 (1:1000) staining was added in the last wash following the secondary antibody incubation. The primary antibody used was KAP1 (1:500) to determine the presence of human sequences. Antibody was defined to have reactivity only with human cells and presented a 50% identity in Needleman-Wunsch alignment with chicken KAP1 sequence becoming a suitable antibody to avoid crossreactivity. Slices were mounted onto a glass slide using mounting media and left to dry for 48h prior to imaging with a confocal microscope. The percentage of positive cells were counted using ImageJ and normalised against the total number of cells.

Statistical analysis

Statistical analyses and graphs were performed using GraphPad Prism v.10.3.1. Comparisons were performed using unpaired t test, one or two-way ANOVA with appropriate multiple comparisons testing, or Kruskal-Wallis test. $P < 0.05$ was considered statistically significant. P values obtained from the GEPIA2 database are presented with 2 decimal places while p values obtained from GraphPad statistical analysis will be presented with 4 decimal places.

RESULTS

Multi-database analysis links CXCL1 to inflammation, triple-negative breast cancer, and patient survival

DisGeNET analysis linked CXCL1 to inflammatory and neutrophil associated disease processes (Fig. 1a,b and SI3 Table 2,3). Analysis of CXCL1 mRNA expression in cancer patient datasets using the GEPIA2 database [18] revealed that across cancers, CXCL1 showed tumour-type-dependent differences between malignant and normal tissues (Fig. 1c,d and SI1 Fig.S1a). In breast cancer, CXCL1 was lower in tumour than normal tissue and decreased with advancing stage (Fig. 1e,f). Kaplan-Meier survival analyses revealed that in TNBC, patients with high CXCL1 expression presented a statistically significantly increased overall survival compared with the patient cohort separated based on low levels of CXCL1 expression (log-rank p = 0.02; HR = 0.29) (Fig. 1g). Similarly, in HER2-positive subtype CXCL1 high expression correlates with improved survival (log-rank p = 0.04; HR = 0.31) (Fig. 1h and SI1 Fig.S1b) in contrast to much lower statistical association between expression and outcome considering luminal A and luminal B subtypes (log-rank p = 0.57; log-rank p = 0.46) (Fig. 1i,j and SI1 Fig.S1b).

To better understand the distribution of CXCL1 expression across different breast cancer subtypes, we analysed the publicly available single-cell RNA-sequencing dataset (GSE176078), which includes 130,246 single cells from 26 primary tumours (11 ER+, 5 HER2+, and 10 TNBCs). CXCL1 expression was increased in TNBC compared to HER2 + and ER+ tumours, showing enrichment in cancer epithelial cells and cancer-associated fibroblasts (CAFs). In contrast, myeloid cells showed comparatively low CXCL1 expression across all subtypes (Fig. 1k). The distribution of CXCL1 expression within the CXCL1-positive cell population revealed a continuous distribution of CXCL1 expression rather than distinct clustered populations in both CAFs and cancer epithelial cells (Fig. 1l and SI1 Fig.S1c). To identify possible biological processes associated with high CXCL1 expression levels, gene ontology enrichment analysis was performed on cancer epithelial cells expressing high levels of CXCL1 (above the 90th percentile of all positive cells) compared to cells with undetectable levels of CXCL1. This analysis revealed an enrichment of processes related to inflammatory and chemokine-associated signalling (Fig. 1m and SI3 Table 6). Enrichment analysis in high-CXCL1 expressing CAFs revealed enrichment of similar inflammatory and cytokine-related pathways, supporting the existence of an inflammatory transcriptional programme associated with high CXCL1 expression in both tumour and stromal cells (SI1 Fig.S1d-j and SI3 Table 6).

Spatial transcriptomic data from the same dataset was used to investigate the spatial organisation of high CXCL1 expressing cells. Spots were grouped based on transcriptional similarity into 7 clusters (Fig. 1n). Gene analysis classified the clusters (0, 1, 2, 3, 4, 5, 6) in epithelial-rich, epithelial-rich associated with inflammation, stromal-inflammatory region, stromal-rich, inflamed stroma, immune-rich and tumour-stroma interface respectively (Fig. 1o and SI1 Fig.S1k). Mapping of high CXCL1 expression spots revealed that high CXCL1 cells are not localised within a specific cluster, suggesting a role of CXCL1 across distinct microenvironments and cell types (Fig. 1p and SI1 Fig.S1l).

CXCL1 silencing promotes a more aggressive breast cancer phenotype in vitro

Based on the cancer patient data analysis and characterisation (Fig. 1) we hypothesised a potentially beneficial role for CXCL1 in triple-negative breast cancer. As a cell model we used the TNBC cell line, MDA-MB-231 which has a significantly higher level of CXCL1 expression compared to hormone receptor positive MCF7 cells (Fig. 2a) and a clear vesicle localisation of the protein as expected for a secretory chemokine (Fig. 2b). Silencing of CXCL1 using siRNA (siCXCL1 and siCXCL1–B) resulted in a significant mRNA (75 and 50%) and protein downregulation compared to the control (Fig. 2c-e and SI1 Fig.S2a). CXCL1 downregulation resulted in a significant increase in the invasion capacity (Fig. 2f), migration and clonogenic capacities (Fig. 2g,h). The same trend was observed silencing CXCL1 with a different siRNA sequence (siCXCL1-B) (Fig. 2f,g and SI1 Fig.S2b,c). Cell cycle analysis showed no alterations or enrichments in cell cycle phase, proliferation or arrest comparing control and siCXCL1 conditions which may account for the increased metastatic and invasive potential (Fig. 2i and SI1 Fig.S2d-g). The growth of breast cancer cells in 3D non-adherent conditions as spheroids is a well established model which more closely recapitulates metastatic disease [19]. Indeed analysis of MDA-MB-231 global RNA sequencing data comparing 2D and 3D cultures (GSE130590) revealed 4084 genes differentially

expressed (padj ≤ 0.001, |log2FC|≥ 1.0) between the culture conditions (Fig. 3a and SI3 Table 5). The upregulation of Mucin (MUC5A), and the downregulation of KISS1 in 3D compared to 2D cell culture conditions noted in the RNAseq (Fig. 3a) was reproduced in MDA-MB-231 3D spheroid cultures (Fig. 3b). Spheroid cultures present a more aggressive phenotype compared to 2D culture conditions that could be related to the basal CXCL1 levels. Interestingly, CXCL1 mRNA levels are significantly higher in 3D cultures compared to 2D monolayers (Fig. 3c). CXCL1 receptor expression was quantified using RT-qPCR to determine variations in their expression. Expression in 2D cultures was significantly higher compared to 3D cultures (Fig. 3d). Similar to the effects observed in 2D (SI1 Fig.S3a) knockdown of CXCL1 in this model showed no visual changes in morphology or spheroid structure but revealed a tendency to form larger spheroids (Fig. 3e and SI1 Fig.S3a). Consistent with the cell cycle analysis in 2D (Fig. 2i) spheroids on day 6 did not present increased mortality or apoptosis which may account for the change in size (Fig. 3f,g). Further in depth spheroid analysis revealed that the effect on spheroid area and size continues even after the siRNA is cleared (SI1 Fig.S3b-d). No statistically significant variations in the eccentricity of the spheroids were identified in the different conditions (SI1 Fig.S3c).

CXCL1 knockdown promotes tumour growth, vascularization, and dissemination in the CAM model

Since their initial description [20] chorioallantoic membrane (CAM) assays have provided a relatively inexpensive, rapid and effective research model in particular for the study of tumour formation and dissemination [21]. The CAM membrane from the chicken embryo acts as a bioreactor allowing tumour cells to proliferate and migrate to peripheral tissues. To transplant MDA-MB-231 cells in the CAM model the experimental procedure had a total duration of 14 days, during which time chicken embryos were handled as described in Section 2.9 (Fig. 4a). Tumours in all conditions in general varied in size however tumours derived from CXCL1 KD cells presented a clear and significant increase in size compared with the control (siCTRL) group (Fig. 4b). Tumours harvested presented visual changes in morphology depending on the experimental group (Fig. 4b). Generally, tumours presented different degrees of vascularization as well as different shapes and variations in the transparency and colour among the different conditions. Tumours from siCXCL1 MDA-MB-231 cells show what appears to be an increase in blood vessel formation surrounding the transplanted tumour and an apparent increase in angiogenesis that supports the tumour development inside of the silicone ring (Fig. 4c,d). RNA was extracted from the CAM tissue and RT-qPCR revealed the detection of human ALU sequences in the tumour sections in all conditions except the negative control (Naked egg, where no breast cancer cells were transplanted). For peripheral organs, CXCL1 KD showed an increased presence of human sequences in fragments from the liver and the lungs (Fig. 4e) indicating that MDA-MB-231 cells have the capacity to leave the graft site and migrate through the developing embryo a process which is clearly comparable as a model for cancer metastatic spread and that this metastatic capacity of the TNBC cells is further enhanced when CXCL1 levels are reduced. Immunohistochemistry was performed to support the findings obtained through RT-qPCR that firstly MDA-MB-231 cells migrate inside the growing embryo to peripheral organs and further to this that samples obtained from CXCL1 KD treated CAM showed a significantly higher percentage of

positive human cells compared to control (Fig. 4f,g). Interestingly, the expression and IF results indicate that in control conditions most of the cells are localised to the graft site close to the CAM (control and tumour) whereas CXCL1 KD cells were more spread to the distal organs.

To gain insight into the molecular mechanisms and potential pathways driven by CXCL1 in TNBC migration we explored the transcriptional programmes associated with high CXCL1 expression. Differential expression analysis using the single-cell RNA-sequencing dataset (GSE176078) was carried out comparing cancer epithelial cells and CAFs grouping based on either positive or negative CXCL1 populations. The top 15 upregulated and downregulated genes in cancer epithelial cells were identified (Fig. 4h and SI3 Table 7). CXCL1-high cells showed an increased expression of inflammatory-associated genes such as CXCL8, S100A6, S100A8, S100A9 and CXCL2, concomitantly with a decreased expression of genes associated with cell adhesion and differentiation, including BCAM, CLDN3, and DCXR. Top 15 upregulated and downregulated genes in CAFs were also analysed (SI1 Fig.S4a). Similarly in CAFs, CXCL1-high cells showed increased expression of inflammatory genes such as, CXCL2, CXCL3, and PTGS2, while CXCL1-negative CAFs showed high expression of extracellular matrix and stromal-associated genes such as COL1A1, COL1A2, COL3A1 and SPARC.

To characterise transcriptional programmes associated with the micro-environment of high-CXCL1 expression spots (above the 90th percentile of all positive cells) in the spatial transcriptomic dataset, we examined selected epithelial, mesenchymal, immune, and inflammatory-associated markers (Fig. 4i and SI3 Table 8). The immune panel revealed elevated expression of CD163 and S100A8 in CXCL1 high spots. Only ITGA6 expression was increased within the CXCL1 high spots in the stemness panel; however the stem markers VIM, ALDH1A1, KRT14 and CD44 clearly increased when CXCL1 was absent (Fig. 4i, right panel). Similarly, EMT regulators, EPCAM, CDH1, and VIM were also elevated when CXCL1 is low. CXCL1 expression showed weak positive spatial correlations with inflammatory and myeloid-associated markers, including CXCL2, LYZ, NFKBIA, IL1B, TNF, PTPRC, and ITGAM (SI1 Fig. S4b).

DISCUSSION

In this study, we describe a context-dependent role for CXCL1 in triple-negative breast cancer. By using *in vitro* and *in vivo* techniques together with patient-derived data, we provide evidence to support a novel driver in TNBC where reduced CXCL1 expression is associated with increased tumour aggressiveness traits supporting the possibility of a context-dependent tumour-protective behaviour.

CXC chemokines, including CXCL1, have been associated with tumour progression. For instance, CXCL1-CXCR2 axis has been reported to have pro-tumourigenic effects in several cancer types such as colorectal and oesophageal squamous cell carcinoma [22, 23]. Previous studies have reported pro-oncogenic roles for CXCL1 by promoting cancer progression and favouring lung metastasis in breast cancer through recruitment of tumour cells and neutrophils to metastatic niches [24]. However, our results presented that transient silencing of CXCL1 in MDA-MB-231 resulted in a consistent increase in migratory, invasive and clonogenic capacity (Fig. 2f-h). These phenotypic changes were complemented

with spheroid cultures, where downregulation of CXCL1 promoted the formation of larger spheres (Fig. 3e), suggestive of enhanced aggressive behaviour by affecting proliferation, survival and stem-like properties [25]. In addition, in CAM assays, CXCL1 KD tumours were larger and presented increased migration (Fig. 4b,f,g), suggesting that the observed phenotype *in vitro* may extend to this *in vivo* model. Although the CAM assay does not fully reproduce the stromal and immune complexity of the tumour microenvironment, the literature reinforces this model as a reliable model for investigating breast cancer [26]. Our findings add a new layer of complexity to CXCL1, suggesting that in this context it may behave as a regulatory signal that restrains excessive tumour progression. One possible explanation is that CXCL1 may have driving distinct effects via the formation of autocrine positive feedback loops. Another explanation may be that the biological effect of CXCL1 is not only shaped by its expression level, but also by receptor usage and its consequent downstream signalling. Recent literature has shown that different CXCR2 ligands can trigger distinct signalling cascades, suggesting the use of the canonical receptor alone does not lead to identical downstream responses [27]. Moreover, CXCR2 has been described as a highly promiscuous receptor [28], raising the possibility that differences in the receptor availability or binding mode could modulate CXCL1 signalling toward a tumour-restraining outcome in some specific contexts. Interestingly, previous studies have demonstrated that CXCL1 expression can also be regulated through post-transcriptional mechanisms. For example, adenoviral E1A induces CXCL1 expression through mRNA stabilisation rather than transcriptional activation, highlighting how CXCL1 can participate in distinct biological programmes depending on cellular context [29]. Together, these observations support the concept that the biological consequences of CXCL1 signalling are determined not only by its expression level but also by the molecular networks that regulate and respond to it. For example, a context-dependent situation has been described in breast cancer, where CXCL13 expression in 4T1 TNBC tumour microenvironment promotes anti-tumour activity in immune-competent mice [30] indicating how chemokine signalling can have a tumour-suppressing effect in a favourable immune context.

This complexity is particularly relevant in TNBC, which is itself a highly heterogeneous subtype as it includes biological changes going from mesenchymal programmes such as ECM remodelling to immune-inflamed phenotypes [31, 32]. In fact, MDA-MB-231 is a mesenchymal-like, highly invasive TNBC model that can occur in either immune activated and immune suppressed states affecting chemokine dependence and receptor-context signalling [33]. Following this idea, a limitation of the study is the use of MDA-MB-231 cell line, which represents one TNBC context and may not reflect the biological diversity across the clinical cases. For this reason, studies in other TNBC models and patient-derived samples will be needed to clarify the conditions under which CXCL1 may promote a tumour-restraining effect.

Spatial transcriptomics analysis showed CXCL1 high spots colocalise with different genetic targets. In the immune cell panel, CD163 corresponds to a specific marker of monocytes and macrophages [34]. S100A8 is also a marker for inflammatory responses, secretion and cell migration [35]. This marker is associated with poor prognosis in breast cancer [36]. This data suggest that cells pertaining to high CXCL1 spots may be inflammation-associated as the top targets are for macrophages and inflammatory modulation. In the stemness panel, the cell motility and cell-cell communication marker ITGA6 showed

an increase in expression [37, 38] when CXCL1 is high in contrast to CD44, VIM and KRT14 which are elevated when CXCL1 is lost, indicating perhaps that the protective effect of CXCL1 expression is due to the downregulation of stem and EMT genes such as CD44, VIM, EPCAM and CDH1. Single cell analysis performed in cancer epithelial cells from the TNBC subtype revealed upregulated genes and several candidates associated with inflammation and stress response. Firstly, ANXA1 encodes Annexin I that is described to have an anti-inflammatory role and act as a negative regulator of tumour progression and immune evasion [39].

Other interesting targets include the upregulation of CXCL8 and CXCL2 which may support the inflammatory behaviour surrounding CXCL1 high cells. CXCL8, or IL-8, is associated with poor prognosis in TNBC [40] and shares the receptor with CXCL1. As discussed in the introduction, standard therapies and ongoing research aim to inhibit the CXCR2 receptor to block the effect of the chemokines [41] in cancer, highlighting the importance of understanding the mechanism and crosstalk between chemokines and receptors in cancer. These proteins may support the inflammatory environment surrounding CXCL1 high tumour-suppressing cancer cells, indeed CXCL2, has been shown to play a role in CAF induction and activation in TNBC [42]. S100A8/S100A9 belong to the S100 proteins that, among other diseases, are highly related to cancer biology. In breast cancer, its expression is related to MDSC recruitment inducing immune suppression and it has been shown to activate MAPK and NF-kB pathways through TLR4 and RAGE receptors in an autocrine manner upregulating genes associated with tumour invasion and growth [43]. Top downregulated genes did not belong to an inflammatory signature as the top upregulated. In general, top downregulated genes are metabolic regulators and structural proteins. In detail, CLDN3 is a structural protein significantly associated with poor overall survival and disease free survival in TNBC and is correlated to nuclear expression of Sip1 (ZEB2) transcription factor [44]. Both upregulated and downregulated hits are essential genes in human development. However, further investigation is required to determine its role or not in the CXCL1 mechanism.

Our findings suggest that, in an aggressive TNBC context, endogenous CXCL1 may act as a regulatory signal that restrains excessive tumour progression. Consequently, therapeutic approaches are targeting proinflammatory chemokines and their receptors causing their inhibition. This strategy may not be universally beneficial across all TNBC contexts or disease stages but rather blocking the CXCL1-CXCR2 pathway may be beneficial in breast cancer situations where this mechanism supports inflammation that promotes tumour growth or resistance to treatment [45]. Simultaneously, findings of increased compensatory chemokines in response to CXCR2 antagonism indicate that these strategies may need meticulous, context-dependent assessment instead of widespread use in different TNBC contexts [46].

The hypothesised protective role of CXCL1 was supported by analyses of patient datasets showing that low CXCL1 expression was associated with reduced overall survival in TNBC (Fig. 1g). These data increase the potential clinical relevance of our findings although the value of CXCL1 expression as a prognostic biomarker or treatment-stratification marker would require independent validation. Despite the pro-aggressive phenotype driven by CXCL1 silencing, the mechanisms underlying this dual role remain to be elucidated. Furthermore, transient silencing is a further limitation of the study, and future

work should include stable CXCL1 knock-out cell line employing techniques such as CRISPR-Cas9 gene editing. In addition, further work should define the receptor context, downstream effectors and pathways implications through CXCL1 execute these context-dependent effects.

CONCLUSION

In conclusion, our findings suggest that GROa/CXCL1 may have a context-dependent protective role in some TNBC contexts, challenging the current view of GROa/CXCL1 as a tumour promoting factor. These results highlight the complexity of chemokine signalling in cancer and highlight the importance of tumour context when considering therapeutic strategies targeting inflammatory pathways.

Declarations

Ethics approval and consent to participate:

Experimentation protocol does not require ethical approval according to Spanish and European legislation (RD 53/2013 and Directiva 2010/63/UE) as chicken embryos are not considered experimentation animals until embryonic developmental day 21.

Competing interests

The authors declare that they have no competing interests.

Clinical trial number: Not applicable.

Funding

This work was supported by the Ramón y Cajal Fellowship (RYC2021-030923-I) funded by MCIN/AEI/10.13039/501100011033 awarded to RW and by the AIRC IG-2022 grant 27712 awarded to R.F.

Author Contributions

Clàudia Martínez Miralles: Experimental design, manuscript and draft preparation, experimental data acquisition, figure and table preparation and manuscript revision and editing. Evangelos Manousakis: Review and draft preparation, experimental data acquisition, figure and table preparation and manuscript revision and editing. Cristina Moreta-Moraleda: Review and draft preparation, experimental data acquisition, figure and table preparation and manuscript revision and editing. Houda Baccara: Review and draft preparation, experimental data acquisition, figure and table preparation Luke Mahon: Experimental data acquisition, figure and table preparation Laia Liñán Franquet: Experimental data acquisition, figure and table preparation. Anna Tomás Pujolà: Experimental data acquisition, figure and table preparation. Montserrat Montañes i Albó: Experimental data acquisition, figure and table preparation. Roberto Ferrari: manuscript revision and editing and funding acquisition. Roni H. G. Wright:

Study and experimental design, review and draft preparation, manuscript revision and editing and funding acquisition. All authors approved the final manuscript.

Availability of data and materials

The datasets used in this study supporting the conclusions of this article were published and are available in the Gene Expression Omnibus repository, GSE176078 (https://www.ncbi.nlm.nih.gov/geo/query/acc.cgi?acc=GSE176078) and Zenodo repository, https://doi.org/10.5281/zenodo.4739739 (https://zenodo.org/records/4739739).

Consent for publication

Not applicable

Acknowledgments

The authors would like to thank all members of the Department of Biomedical Sciences, Faculty of Medicine and Health Sciences, Universitat Internacional de Catalunya, Barcelona, Spain.

References

1. Bray F, Laversanne M, Sung H et al (2024) Global cancer statistics 2022: GLOBOCAN estimates of incidence and mortality worldwide for 36 cancers in 185 countries. CA Cancer J Clin 74:229–263. https://doi.org/10.3322/caac.21834
2. Xiong X, Zheng L-W, Ding Y et al (2025) Breast cancer: pathogenesis and treatments. Signal Transduct Target Ther 10:49. https://doi.org/10.1038/s41392-024-02108-4
3. Zagami P, Carey LA (2022) Triple negative breast cancer: Pitfalls and progress. NPJ Breast Cancer 8:95. https://doi.org/10.1038/s41523-022-00468-0
4. Bianchini G, De Angelis C, Licata L, Gianni L (2022) Treatment landscape of triple-negative breast cancer - expanded options, evolving needs. Nat Rev Clin Oncol 19:91–113. https://doi.org/10.1038/s41571-021-00565-2
5. Hanahan D, Weinberg RA (2011) Hallmarks of cancer: the next generation. Cell 144:646–674. https://doi.org/10.1016/j.cell.2011.02.013
6. Mackay CR (2001) Chemokines: immunology's high impact factors. Nat Immunol 2:95–101. https://doi.org/10.1038/84298
7. Barkaway A, Rolas L, Joulia R et al (2021) Age-related changes in the local milieu of inflamed tissues cause aberrant neutrophil trafficking and subsequent remote organ damage. Immunity 54:1494–1510e7. https://doi.org/10.1016/j.immuni.2021.04.025
8. Yang J, Jin L, Kim HS et al (2022) KDM6A Loss Recruits Tumor-Associated Neutrophils and Promotes Neutrophil Extracellular Trap Formation in Pancreatic Cancer. Cancer Res 82:4247–4260. https://doi.org/10.1158/0008-5472.CAN-22-0968

9. Zhang W, Wu Q, Wang C et al (2018) AKIP1 promotes angiogenesis and tumor growth by upregulating CXC-chemokines in cervical cancer cells. Mol Cell Biochem 448:311–320. https://doi.org/10.1007/s11010-018-3335-7
10. Li J, Wang S, Wang N et al (2021) Aiduqing formula inhibits breast cancer metastasis by suppressing TAM/CXCL1-induced Treg differentiation and infiltration. Cell Commun Signal 19:89. https://doi.org/10.1186/s12964-021-00775-2
11. Yang X, Chen X, Zhang S et al (2023) Collagen 1-mediated CXCL1 secretion in tumor cells activates fibroblasts to promote radioresistance of esophageal cancer. Cell Rep 42:113270. https://doi.org/10.1016/j.celrep.2023.113270
12. Alexander E, Hildebrand DG, Kriebs A et al (2013) IκBζ is a regulator of the senescence-associated secretory phenotype in DNA damage- and oncogene-induced senescence. J Cell Sci 126:3738–3745. https://doi.org/10.1242/jcs.128835
13. Liu G, Rui W, Zheng H et al (2020) CXCR2-modified CAR-T cells have enhanced trafficking ability that improves treatment of hepatocellular carcinoma. Eur J Immunol 50:712–724. https://doi.org/10.1002/eji.201948457
14. Ciummo SL, D'Antonio L, Sorrentino C et al (2021) The C-X-C Motif Chemokine Ligand 1 Sustains Breast Cancer Stem Cell Self-Renewal and Promotes Tumor Progression and Immune Escape Programs. Front Cell Dev Biol 9:689286. https://doi.org/10.3389/fcell.2021.689286
15. Wang X, Wang Z, Liao Q et al (2025) Spatially resolved atlas of breast cancer uncovers intercellular machinery of venular niche governing lymphocyte extravasation. Nat Commun 16:3348. https://doi.org/10.1038/s41467-025-58511-0
16. Wu SZ, Swarbrick A (2021) A single-cell and spatially resolved atlas of human breast cancers | spatial transcriptomics data. https://doi.org/10.5281/zenodo.4739739. Zenodo
17. Piñero J, Corvi J, Rykova N et al (2026) DISGENET: Accelerating Data-Driven Discovery in Disease Genomics and Therapeutic Development. https://doi.org/10.64898/2026.01.05.697749. BioRxiv
18. Tang Z, Kang B, Li C et al (2019) GEPIA2: an enhanced web server for large-scale expression profiling and interactive analysis. Nucleic Acids Res 47:W556–W560. https://doi.org/10.1093/nar/gkz430
19. Ishiguro T, Ohata H, Sato A et al (2017) Tumor-derived spheroids: Relevance to cancer stem cells and clinical applications. Cancer Sci 108:283–289. https://doi.org/10.1111/cas.13155
20. Chu P-Y, Koh AP-F, Antony J, Huang RY-J (2022) Applications of the chick chorioallantoic membrane as an alternative model for cancer studies. Cells Tissues Organs (Print) 211:222–237. https://doi.org/10.1159/000513039
21. Faehling T, Reiff T, Schumacher B et al (2026) Beyond the mouse: 3R-guided alternative animal models transforming cancer research. Mol Cancer 25. https://doi.org/10.1186/s12943-026-02601-0
22. Chen H, Pan Y, Zhou Q et al (2022) METTL3 Inhibits Antitumor Immunity by Targeting m6A-BHLHE41-CXCL1/CXCR2 Axis to Promote Colorectal Cancer. Gastroenterology 163:891–907. https://doi.org/10.1053/j.gastro.2022.06.024

23. Xiong G, Chen Z, Liu Q et al (2024) CD276 regulates the immune escape of esophageal squamous cell carcinoma through CXCL1-CXCR2 induced NETs. J Immunother Cancer 12. https://doi.org/10.1136/jitc-2023-008662
24. Cao L, Li Y, Ou M et al (2025) Mesenchymal stromal cells highly expressing Sca-1 promote breast cancer lung metastasis through recruiting myeloid cells. Cell Death Dis 16:507. https://doi.org/10.1038/s41419-025-07845-0
25. Mungai RW, Hartman RJ, Jolin GE et al (2024) Towards a more objective and high-throughput spheroid invasion assay quantification method. Sci Rep 14:31007. https://doi.org/10.1038/s41598-024-82191-3
26. Ranjan RA, Muenzner JK, Kunze P et al (2023) The chorioallantoic membrane xenograft assay as a reliable model for investigating the biology of breast cancer. Cancers (Basel) 15. https://doi.org/10.3390/cancers15061704
27. Boon K, Vanalken N, Szpakowska M et al (2024) Systematic assessment of chemokine ligand bias at the human chemokine receptor CXCR2 indicates G protein bias over β-arrestin recruitment and receptor internalization. Cell Commun Signal 22:43. https://doi.org/10.1186/s12964-023-01460-2
28. Saha S, Sano FK, Sharma S et al (2025) Molecular basis of promiscuous chemokine binding and structural mimicry at the C-X-C chemokine receptor, CXCR2. Mol Cell 85:976–988e9. https://doi.org/10.1016/j.molcel.2025.01.024
29. Ferrari R, Gou D, Jawdekar G et al (2014) Adenovirus small E1A employs the lysine acetylases p300/CBP and tumor suppressor Rb to repress select host genes and promote productive virus infection. Cell Host Microbe 16:663–676. https://doi.org/10.1016/j.chom.2014.10.004
30. Ma Q, Chen Y, Qin Q et al (2021) CXCL13 expression in mouse 4T1 breast cancer microenvironment elicits antitumor immune response by regulating immune cell infiltration. Precis Clin Med 4:155–167. https://doi.org/10.1093/pcmedi/pbab020
31. Bareche Y, Venet D, Ignatiadis M et al (2018) Unravelling triple-negative breast cancer molecular heterogeneity using an integrative multiomic analysis. Ann Oncol 29:895–902. https://doi.org/10.1093/annonc/mdy024
32. Shiao SL, Gouin KH, Ing N et al (2024) Single-cell and spatial profiling identify three response trajectories to pembrolizumab and radiation therapy in triple negative breast cancer. Cancer Cell 42:70–84e8. https://doi.org/10.1016/j.ccell.2023.12.012
33. García-Areas R, Girard E, Lasla H et al (2026) Wnt signaling promotes inflammation and EMT-associated gene expression in mesenchymal TNBC. Sci Rep. https://doi.org/10.1038/s41598-026-43678-3
34. He K-F, Zhang L, Huang C-F et al (2014) CD163 + tumor-associated macrophages correlated with poor prognosis and cancer stem cells in oral squamous cell carcinoma. Biomed Res Int 2014:838632. https://doi.org/10.1155/2014/838632
35. Hong WC, Lee DE, Kang HW et al (2023) CD74 Promotes a Pro-Inflammatory Tumor Microenvironment by Inducing S100A8 and S100A9 Secretion in Pancreatic Cancer. Int J Mol Sci 24.

https://doi.org/10.3390/ijms241612993

36. Miller P, Kidwell KM, Thomas D et al (2017) Elevated S100A8 protein expression in breast cancer cells and breast tumor stroma is prognostic of poor disease outcome. Breast Cancer Res Treat 166:85–94. https://doi.org/10.1007/s10549-017-4366-6
37. Hoogland AM, Verhoef EI, Roobol MJ et al (2014) Validation of stem cell markers in clinical prostate cancer: α6-integrin is predictive for non-aggressive disease. Prostate 74:488–496. https://doi.org/10.1002/pros.22768
38. Faraldo MM, Romagnoli M, Wallon L et al (2024) Alpha-6 integrin deletion delays the formation of Brca1/p53-deficient basal-like breast tumors by restricting luminal progenitor cell expansion. Breast Cancer Res 26:91. https://doi.org/10.1186/s13058-024-01851-4
39. Al-Ali HN, Crichton SJ, Fabian C et al (2024) A therapeutic antibody targeting annexin-A1 inhibits cancer cell growth in vitro and in vivo. Oncogene 43:608–614. https://doi.org/10.1038/s41388-023-02919-9
40. Vuong NB, Korolkova OY, Izban MG et al (2026) Contribution of Mesenchymal-like and Epithelial Cellular Subsets to Chemotherapy Resistance in Triple-Negative Breast Cancer. Int J Mol Sci 27. https://doi.org/10.3390/ijms27073157
41. Hu X, Xiong Y, Villodre ES et al (2026) Soluble E-cadherin-CXCL1-CXCR2 axis as a therapeutic vulnerability in inflammatory breast cancer brain metastasis. Neuro Oncol 28:1220–1236. https://doi.org/10.1093/neuonc/noag012
42. Hsieh M-Y, Yang C-C, Hsu W-J et al (2026) Piperlongumine suppresses YAP-ET-1-CXCL2 signaling to modulates aggressiveness of triple-negative breast cancer cells. Transl Oncol 66:102700. https://doi.org/10.1016/j.tranon.2026.102700
43. Bresnick AR, Weber DJ, Zimmer DB (2015) S100 proteins in cancer. Nat Rev Cancer 15:96–109. https://doi.org/10.1038/nrc3893
44. Jääskeläinen A, Soini Y, Jukkola-Vuorinen A et al (2018) High-level cytoplasmic claudin 3 expression is an independent predictor of poor survival in triple-negative breast cancer. BMC Cancer 18:223. https://doi.org/10.1186/s12885-018-4141-z
45. Ghallab AM, Eissa RA, El Tayebi HM (2022) CXCR2 Small-Molecule Antagonist Combats Chemoresistance and Enhances Immunotherapy in Triple-Negative Breast Cancer. Front Pharmacol 13:862125. https://doi.org/10.3389/fphar.2022.862125
46. Erin N, Tavşan E, Akdeniz Ö et al (2021) Rebound increases in chemokines by CXCR2 antagonist in breast cancer can be prevented by PKCδ and PKCε activators. Cytokine 142:155498. https://doi.org/10.1016/j.cyto.2021.155498

Figures

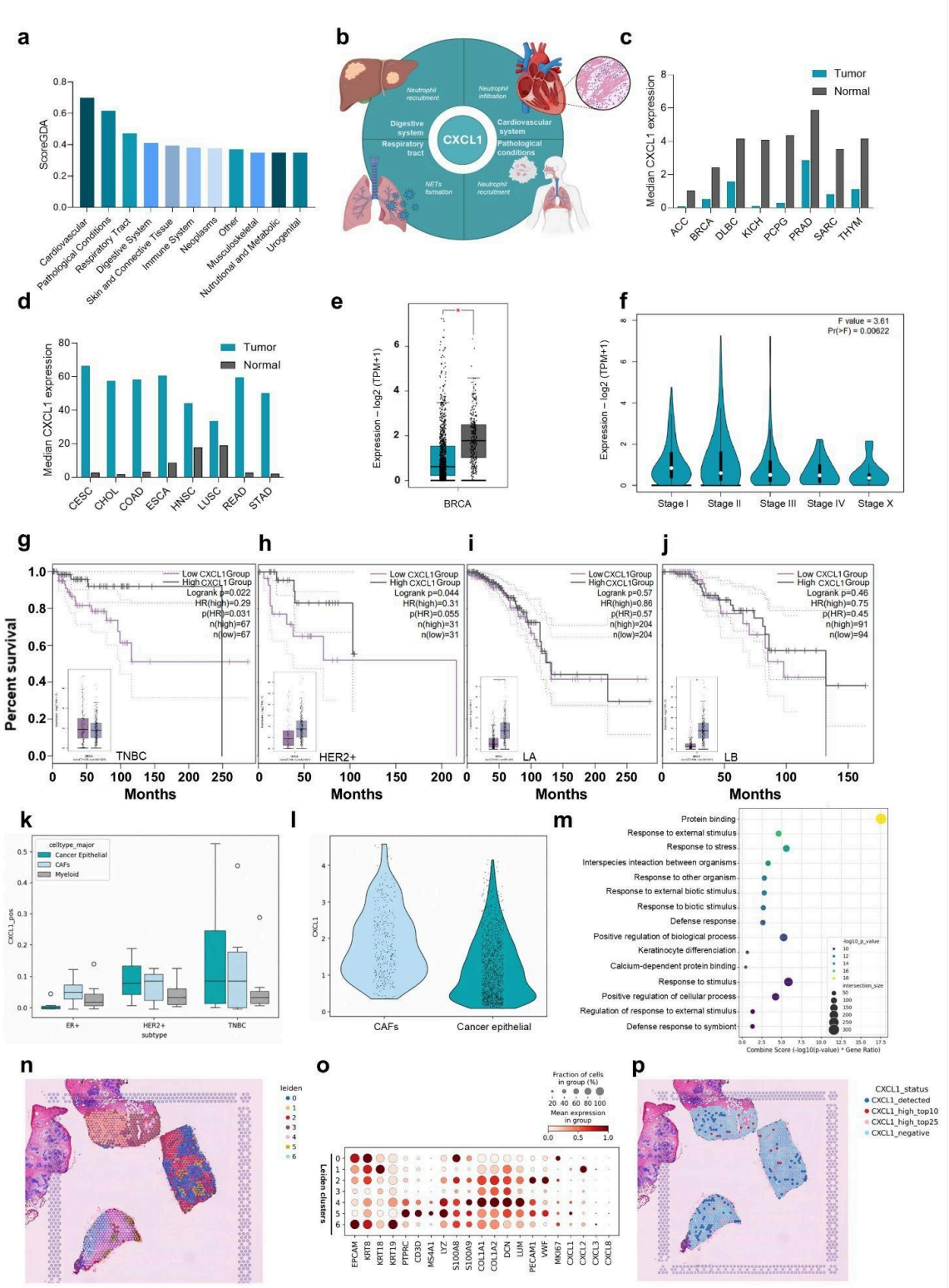


Figure 1

CXCL1 expression in diseases and its variation in expression levels depending on breast cancer subtypes. **(a)** DisGeNET [17] analysis of CXCL1 association with different systems, from higher to lower representation. Data was retrieved from DisGeNET database and values are expressed as ScoreGDA (ScoreGDA=1 highest evidence level, High ≥ 0.3). **(b)** Schematic representation of CXCL1-mediated pathological mechanisms across the top diseases identified by DisGeNET analysis. CXCL1 expression

promotes neutrophil recruitment and infiltration into peripheral tissues and promotes the formation of neutrophil extracellular traps (NETs) in some tissues. **(c,d)** Bar plot representing the median CXCL1 expression in transcripts per million in paired tumour and adjacent normal tissue in different cancer types. Abbreviations in supplementary information 3 Table 4. Data is retrieved from RNA-seq analysis from GEPIA2 [18] **(e)** CXCL1 expression in normal paired to tumour tissue in breast cancer boxplot was generated through GEPIA2 (num(T)=1085; num(N)=291; statistical differences were measured using one-way ANOVA (*p-value cutoff<0.01)). **(f)** Violin plot representing the variation in CXCL1 expression through different stages of the disease. Stage X corresponds to unclassified tissue samples. (Pr(>F)=0.00622; F=3.61) **(g-j)** Kaplan-Meier overall-survival curve from different breast cancer subtypes: triple-negative breast cancer **(g)**, HER2-positive **(h)**, Luminal A **(i)** and Luminal B **(j)** stratified by CXCL1 mRNA expression (lavender=low CXCL1 expression, purple=high CXCL1 expression). The y axis represents the percentage of survival and the x axis the time in months (significant if log-rank $p<0.05$). **(k)**Boxplot obtained from single cell analysis classifying the amount of positive CXCL1 depending on the cancer subtype and the cell type. **(l)**Distribution of the CXCL1-positive cells in the single cell samples in cancer epithelial and CAFs cell types. **(m)** Biological process GO analysis for the CXCL1 positive cells in cancer epithelial major cell types. The size of the dot represents the percentage of genes in the set. **(n)** Spatial transcriptomics analysis from CID44971 TNBC tumour. Architectural distribution of the leiden clusters according to genetic signature. **(o)** Dot blot representing the characteristic genetic signature of each leiden cluster. **(p)**Distribution of CXCL1 expression in the tumour sample in represented sections as CXCL1 negative, CXCL1 positive, top 25 sections with high CXCL1 and the top 10 sections with high CXCL1

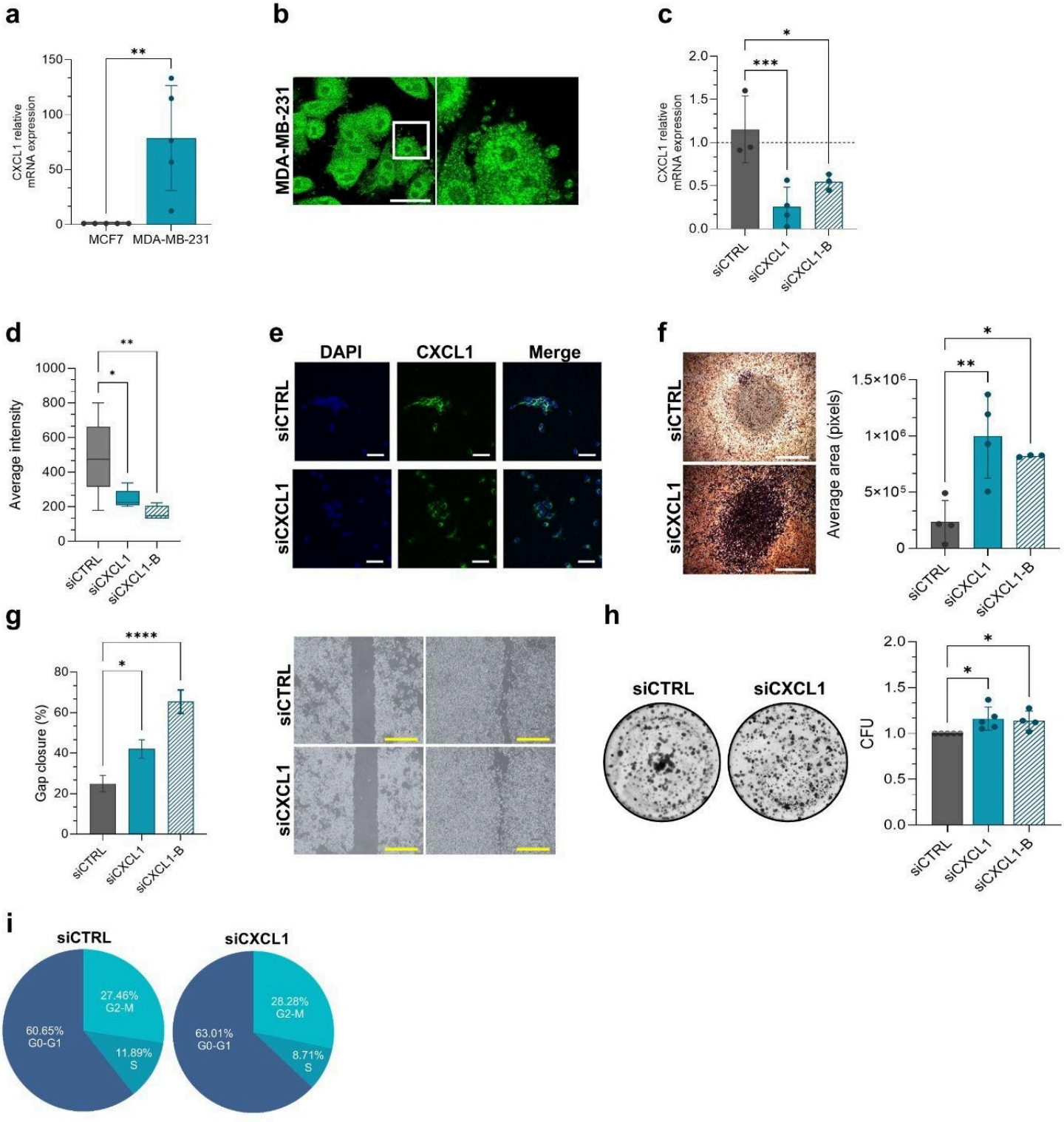


Figure 2

CXCL1 transient knock-down in TNBC cell line increases the invasive and proliferative behaviour showing a more aggressive cancer signature. **(a)** CXCL1 mRNA expression levels in MDA-MB-231 and MCF7 cell lines. (Unpaired t test; N=5; **p=0.0066) **(b)** Representative images of immunofluorescence analysis of CXCL1 protein levels in MDA-MB-231. Zoom section showing vesicle formation in MDA-MB-231 cell line. Scale bar = 40 μm; magnification = 63x. **(c)** CXCL1 mRNA expression levels in MDA-MB-231 after knock-

down using siRNA compared with the control (siCTRL). Transient downregulation was performed with two different siRNA sequences (siCXCL1-1 and siCXCL1-B) (Ordinary one-way ANOVA; N=4; ***p=0,0008; *p=0.0165). **(d-e)** Quantification of CXCL1 protein average intensity in immunofluorescence comparing knock-down with the control condition (siCTRL). Cell nuclei were stained using DAPI and CXCL1 stained in green. Scale bar = 25 um (Ordinary one-way ANOVA, N=5; *p=0.0350; **p=0.0098). For quantification of the signal intensity, more than 100 nuclei were used to assure reliability **(f)** Brightfield images (left) and quantification (right) of the invaded cells comparing siCXCL1 with control conditions. Scale bar = 300 µm (Ordinary one-way ANOVA; N=6; **p=0.0028; *p=0.0243). **(g)** Migration gap brightfield images (right) and quantification (left) of the percentage of gap closure 48h after the scratch was created comparing CXCL1 knock-down with control conditions. (Ordinary one-way ANOVA; N=12; *p=0.0359, ****p<0.0001). **(h)** Colony images (left) and quantification (right) of the number of colony formation units (CFU) comparing siCXCL1 and siCTRL conditions (Kruskal-Wallis test; N=5; *p=0.0108; *p=0.0278). **(i)** Cell cycle analysis comparing the transfection conditions

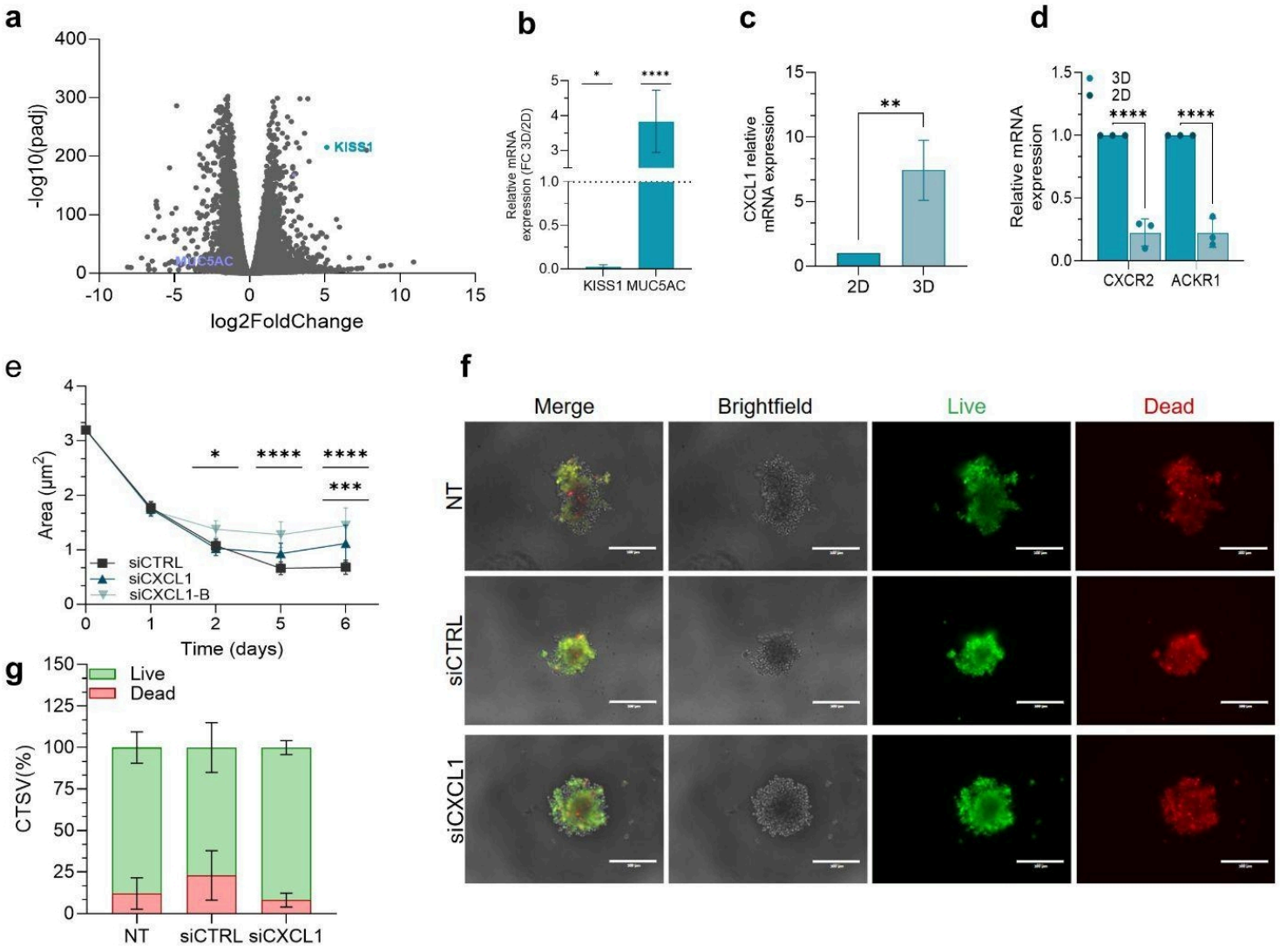


Figure 3

CXCL1 knock-down drives the formation of bigger spheroids in 3D cultures. **(a)**Volcano plot from the analysis of an RNA sequencing database representing expression markers for MDA-MB-231 cell lines in 2D (blue) vs. 3D (purple). **(b)**mRNA expression levels in MDA-MB-231 comparing the expression of MDA-MB-231 specific cancer stem cells markers (MUC5AC, KISS1) in monolayer against 3D cultures (Two-way ANOVA; N=3; *p=0.0194, ****p<0.001). **(c)** CXCL1 mRNA expression levels in MDA-MB-231 comparing monolayer culture (2D) and non-adherent culture (3D) (Unpaired t test; N=3; **p=0.0087). **(d)** mRNA expression levels of CXCL1 receptors CXCR2 and ACKR1 comparing 2D and 3D cultures in MDA-MB-231 cell line (Two-way ANOVA; N=3; ****p=<0.001). **(e)**Normalized spheroid area from spheroids originated from monolayer CXCL1 KDs or control conditions (Two-way ANOVA; N=10; **p=0.0012, ***p=0.0002, ****p=<0.001). **(f,g) (f)** Representative images from the live signal (green),dead signal (red), the bright-field image (spheroid) and the merging of all three channels in the different transfection conditions. Scale bar = 300 µm. **(g)** Quantification of the Live/Dead staining in the different transfection conditions on spheroid growth day 2. Corrected total spheroid values of the spheroids (CTSV) was measured for each condition (Two-way ANOVA; N=4; *ns*)

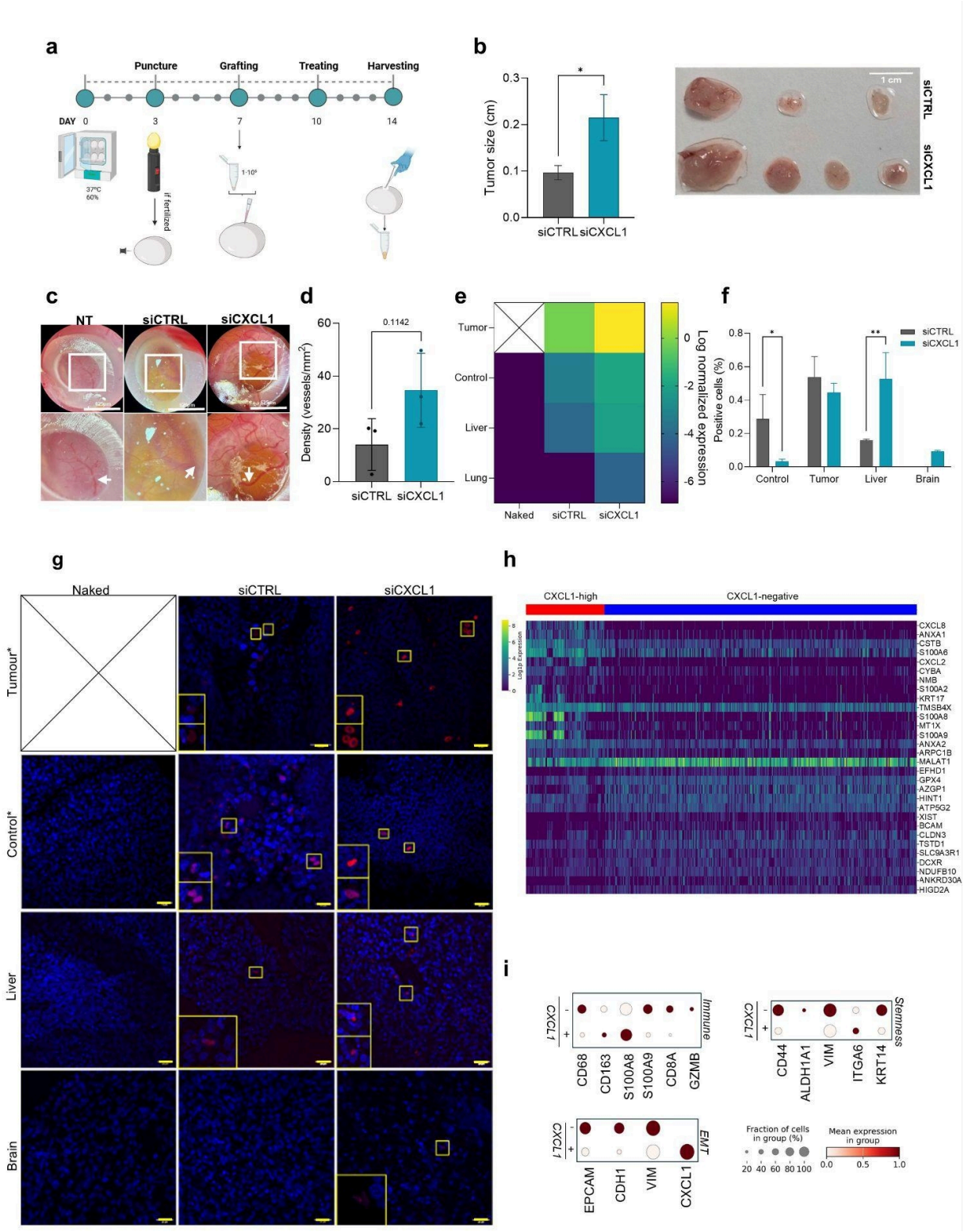


Figure 4

In vivo, CXCL1 knock-down increases aggressive phenotype by increasing tumour size and metastasis. **(a)** Schematic representation of the workflow used *in ovo*CAM assay. **(b)** Image of the Tumours harvested from the CAM on EDD14. Scale bar = 1 cm. Quantification of the tumour area comparing the transfection conditions (Ordinary one-way ANOVA; N=3 ; *p=0.0170). **(c)**Representative images from Tumours located in the CAM comparing different conditions: wt MDA-MB-231 (NT), control condition

(siCTRL) and knock-down CXCL1 (siCXCL1). Scale bar = 625 µm. **(d)** Quantification of the vessel density identified in the different tumour images (Welch t test; N=3; *ns*). **(e)**Heatmap showing calculated human signal in CAM samples (tumour and control) and peripheral organs samples (liver and lung) harvested from the chicken embryos. **(f)**Fluorescent immunohistochemistry quantification of the human cells in several CAM model tissues (CAM or peripheral organs). Labels including "*" refer to tissues that take part of the CAM (control and tumour). Quantification was performed measuring the number of positive human cells per total amount of cells. (Ordinary two-way ANOVA, N=4; **p=0.0050, *p=0.0104) **(g)**Representative images of fluorescent immunohistochemistry staining human targets in different CAM tissues (tumour, CAM control, liver and brain). Scale bar = 19 µm; magnification = 63x. **(h)** Heatmap obtained from single cell analysis comparing top CXCL1 high with a randomised sample of CXCL1-negative to balance biological signification. **(i)**Dot blots created from spatial transcriptomics analysis determining the mean expression of different markers in sections with CXCL1 negative or top 10 high. Dot blots have been classified into immune cells, stemness and EMT markers

Supplementary Files

This is a list of supplementary files associated with this preprint. Click to download.

- Keymessages.pdf
- SupplementaryInformation12and3combined.pdf